Marine ice-sheet dynamics. Part 1.
The case of rapid sliding

CHRISTIAN SCHOOF

Department of Earth and Ocean Sciences, University of British Columbia, 6339 Stores Road,
Vancouver, V6T 1Z4, Canada

Marine ice sheets are continental ice masses resting on bedrock below sea level. Their dynamics are similar to those of land-based ice sheets except that they must couple with the surrounding floating ice shelves at the grounding line, where the ice reaches a critical flotation thickness. In order to predict the evolution of the grounding line as a free boundary, two boundary conditions are required for the diffusion equation describing the evolution of the grounded-ice thickness. By analogy with Stefan problems, one of these conditions imposes a prescribed ice thickness at the grounding line and arises from the fact that the ice becomes afloat. The other condition must be determined by coupling the ice sheet to the surrounding ice shelves. Here we employ matched asymptotic expansions to study the transition from ice-sheet to ice-shelf flow for the case of rapidly sliding ice sheets. Our principal results are that the ice flux at the grounding line in a two-dimensional ice sheet is an increasing function of the depth of the sea floor there, and that ice thicknesses at the grounding line must be small compared with ice thicknesses inland. These results indicate that marine ice sheets have a discrete set of steady surface profiles (if they have any at all) and that the stability of these steady profiles depends on the slope of the sea floor at the grounding line.

1. Introduction

Continental ice sheets, such as those covering Greenland and Antarctica, generally behave as thin viscous films spreading under their own weight, subject to mass gain and loss at their surface owing to snowfall and melting. In their simplest form, mathematical models for ice-sheet flow employ a standard lubrication approximation, which in turn leads to a nonlinear diffusion equation for the evolution of the ice surface (Fowler & Larson 1978; Morland & Johnson 1980; Hutter 1983). The standard boundary conditions that apply to an ice sheet whose edges rest everywhere on land are that the ice thickness and ice flux vanish simultaneously. These conditions then determine the evolution of the moving boundary of the ice sheet as well as of the ice thickness in its interior.

In other words, when coupled with a suitable prescription for the rate at which ice accumulates at the ice-sheet surface, the standard lubrication (or shallow-ice) approximation for the flow of land-based ice sheets yields a closed model. No further attention need be paid to the detailed mechanics of the ice-sheet margins (see also Fowler 1977). Many mathematical challenges posed by this model are analogous to those encountered in other thin-film flows involving contact lines and can be understood in the framework of parabolic obstacle problems (e.g. Calvo *et al.* 2002). Other

approaches include the study of similarity solutions (e.g. Nye 2000; Bueler *et al.* 2005) and of steady-state surface profiles and their uniqueness and stability (in particular when ice accumulation is dependent on surface elevation, in which case multiple steady-state profiles are possible (see e.g. Fowler & Larson 1980; Wilchinsky 2001).

Marine ice sheets differ from their land-based counterparts because they rest on bedrock below sea level, and their margins are located where the ice becomes thin enough to float on the surrounding ocean waters. More precisely, this location is known in glaciology as the grounding line, and it separates grounded ice from the surrounding floating ice shelves. Unlike the grounded ice sheet, ice shelves experience negligible tangential traction on their lower surfaces. As a result, their flow as they spread under their own weight more closely resembles the flow of viscous jets and membranes than the behaviour of a classical lubrication flow (Morland 1987; MacAyeal & Barcilon 1988). Put another way, ice shelves flow as plug flows in which stresses due to longitudinal stretching are dominant, whereas stresses due to vertical shearing are dominant in grounded ice sheets.

The coupling between the two flows has important consequences for the grounded part of a marine ice sheet. By analogy with the case of land-based ice sheets, a marine-ice-sheet model which is able to predict grounding-line motion requires two boundary conditions at the grounding line. One boundary condition, on the ice thickness, derives naturally from the fact that the ice at the grounding line is at a critical thickness at which it becomes afloat. It is worth underlining that, on its own, this boundary condition is not sufficient to determine the motion of the grounding line (note that claims to the contrary can be found in the glaciological literature, see e.g. Hindmarsh 1996; Hindmarsh & LeMeur 2001; LeMeur & Hindmarsh 2001). The obvious analogy here is with Stefan problems in heat conduction: There, temperature satisfies a diffusion equation in the interior of a solid body and reaches a prescribed value at its surface. An additional condition, the Stefan condition, is required to determine the evolution of this free surface due to melting and solidification. For the classical Stefan problem, this additional boundary condition can be determined through simple considerations of conservation of energy. In the case of a marine ice sheet, it must be determined in a rather more complicated way through the mechanical coupling between sheet and shelf.

The importance of the transition zone between grounded and floating ice in controlling the dynamics of marine ice sheets was pointed out over thirty years ago by Weertman (1974). Nonetheless, there have been only a few serious attempts to construct and solve mathematical models of the transition zone that are able to provide effective boundary conditions for the grounded part of the ice sheet. The main exponents of this work have been Chugunov & Wilchinsky (1996) and Wilchinsky & Chugunov (2001), who have based their model on the assumption that the grounded ice sheet does not slide over its bed, while earlier attempts include those by van der Veen (1985) and Herterich (1987). For steady two-dimensional ice sheets with constant viscosity, the analysis of Chugunov & Wilchinsky yields an additional relationship between ice thickness and ice flux at the grounding line. This supplies the missing Stefan-type condition, which was later used by Wilchinsky (2001) to study the stability properties of steady marine ice-sheet profiles. However, the applicability of their boundary condition to the dynamic case is not immediately obvious, as the boundary-layer problem solved by Chugunov & Wilchinsky (1996) presupposes a steady ice sheet.

Our concern in the present paper will be specifically with dynamic ice sheets which are able to slide and, in fact, in which the sliding of ice is rapid compared with velocities due to vertical shearing. There are two motivations for this approach. First, ice sheets
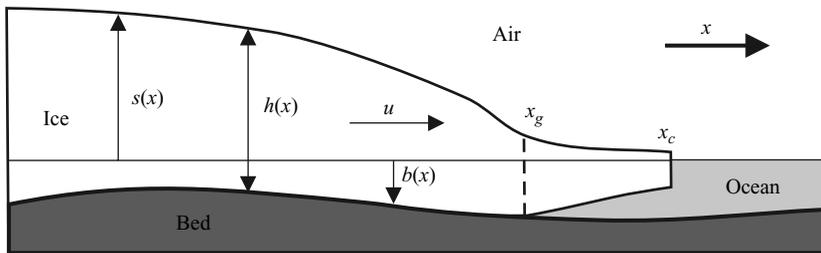
FIGURE 1. Geometry of the problem: s is the surface elevation above sea level, h the ice thickness and b the depth to the sea floor, while x is the horizontal position, $x = x_g$ denoting the grounding line; u is the ice velocity.

typically are able to slide, and the dependence of the relevant boundary conditions at the grounding line on the chosen parameterization of sliding is naturally of interest. Secondly, the assumption that sliding is rapid allows us to employ a simplified, depth-integrated, model for the flow of the coupled ice-sheet–ice-shelf system. As this model is considerably simpler to solve than the full Stokes equations which feature in the work of Chugunov & Wilchinsky, it is hoped that the present approach can fulfil a didactic role in elucidating the basic structure of the transition problem.

The model used here, originally due to Muszynski & Birchfield (1987) and MacAyeal (1989), has been employed in a number of numerical studies of coupled ice-sheet–ice-shelf systems (e.g. Vieli & Payne 2005), the novelty in our paper being a consistent approach using matched asymptotics. The idea of using the model to study ice-sheet–ice-shelf transitions as a boundary-layer problem was developed independently by Hindmarsh (2006), who also obtained some qualitative aspects of the boundary-layer structure described in § 3.3 of paper.

In a companion paper, in preparation, we will present a more detailed derivation of our model from first principles and extend our work to the case of ice sheets whose interior is sliding at a rate comparable with the velocities caused by vertical shearing in the ice, rather than rapidly. The analysis in the companion paper will necessarily be more involved and is motivated to a great extent by the results obtained from the simpler model below.

2. Model

We consider a two-dimensional symmetrical shallow marine ice sheet (figure 1) and suppose that most of its flux is accounted for by sliding at the bed rather than by shearing across the thickness of the ice. Let x denote the horizontal position in the flow direction (with $x = 0$ defining the axis of symmetry), let t denote time and let subscripts x and t signify the corresponding partial derivatives, i.e. $u_x = \partial u / \partial x$ etc. By exploiting the symmetry of the ice sheet, we confine ourselves to $x > 0$ and denote the position of the grounding line at time t by $x_g(t)$, where $x_g > 0$. In addition, we assume that there is a floating ice shelf which extends from the grounding line at $x = x_g(t)$ to a calving front at $x = x_c(t)$, where ice breaks off from the shelf to form icebergs.

Let u be the ice velocity in the x-direction; it is independent of the depth in the ice since we assume that the ice flows approximately as a plug flow. The symbol h will denote the ice thickness, and b the depth of the sea floor below sea level, so the ice-sheet surface elevation is at $s = h - b$ above sea level for the grounded part of the sheet. We assume that any contribution which the ice sheet makes to sea-level change

is small compared with the depth of the bed b and that the bedrock underlying the ice sheet is perfectly rigid. This allows us to prescribe $b(x)$ as a function of position.

The model can then be cast in the following form:

$$\left. \begin{aligned} 2A^{-1/n}\left(h|u_x|^{1/n-1}u_x\right)_x - C|u|^{m-1}u - \rho g h (h-b)_x &= 0 \\ h_t + (uh)_x &= a \\ \rho h &\geqslant \rho_w b \end{aligned} \right\} \text{ on } x \in (0, x_g), \quad (2.1a,b)$$

$$\left. \begin{aligned} 2A^{-1/n}\left(h|u_x|^{1/n-1}u_x\right)_x - \rho(1-\rho/\rho_w)ghh_x &= 0 \\ h_t + (uh)_x &= a \\ \rho h &< \rho_w b \end{aligned} \right\} \text{ on } x \in (x_g, x_c), \quad (2.2a,b)$$

$$\left. \begin{aligned} (h-b)_x &= 0 \\ u &= 0 \end{aligned} \right\} \text{ at } x = 0, \qquad (2.3a,b)$$

$$h, u, u_x \text{ continuous} \quad \text{at} \quad x = x_g, \qquad (2.4)$$

$$\left. \begin{aligned} 2A^{-1/n}h|u_x|^{1/n-1}u_x - \tfrac{1}{2}(1-\rho/\rho_w)\rho g h^2 &= 0 \\ u - v_c(x_c, u, h) &= \dot{x}_c \end{aligned} \right\} \text{ at } x = x_c. \qquad (2.5a,b)$$

Here ρ and ρ_w are the densities of ice and water, respectively, while g is the acceleration due to gravity and $A > 0$ and $n \geqslant 1$ are the usual parameters in Glen's power-law rheology for ice (Paterson 1994, chap. 5). The frictional shear stress at the base of the ice is assumed to behave as $C|u|^{m-1}u$, with C and m positive constants. With $m = 1/n$, a friction law of this type arises when ice slides over rigid bedrock (Fowler 1981); in this case C depends on the small-scale roughness of the ice sheet bed. The quantity a is the rate at which ice accumulates owing to snowfall or is lost (owing to surface melting if a is negative), and we assume that a is given as a function of position and time.

The model represents the following physical components. Equations (2.1) and (2.2) are depth-integrated versions of Stokes' equations, valid for flows in which there is little shear velocity across the thickness of the ice compared with the sliding velocities. Specifically, the first equalities in (2.1) and (2.2) represent force balance, while the second equalities represent conservation of mass. A derivation of these equations for the grounded part of the ice sheet may be found in Muszynski & Birchfield (1987), MacAyeal (1989) and Wilchinsky & Chugunov (2000), and for the floating ice shelves in Morland (1987), MacAyeal & Barcilon (1988), MacAyeal (1996) and Weis, Grieve & Hulter (1999). The inequality constraints in (2.1) and (2.2) signify that the ice thickness in the grounded part of the ice sheet is greater than the thickness at which flotation occurs, while the base of the ice shelf is above the sea floor. The boundary conditions (2.3) are a simple reflection of the symmetry at the centre of the ice sheet. Meanwhile, the continuity requirements (2.4) strictly speaking need to be justified through a boundary-layer description of the transition from grounded to floating ice, which will be supplied in the companion paper. (Note that these continuity requirements differ from those predicted by Chugunov & Wilchinsky (1996), who found a finite jump in u and h across the grounding line. The discrepancy arises because of the assumed rapid sliding motion of the ice sheet in the present paper, which contrasts with the no-slip boundary condition of Chugunov & Wilchinsky. As we shall show in the companion paper, our continuity assumptions actually hold true provided that sliding in the main part of the ice sheet is comparable with vertical shearing and that $m < 2/n$.) Equation (2.2b) represents the rate of mass loss due to iceberg calving at calving velocity v_c at the edge of the ice shelf, where the dot on $\dot{x}_c$

denotes an ordinary derivative with respect to t. Lastly, (2.5*a*) equates an imbalance in hydrostatic pressures in water and ice, which arises because of the buoyancy of ice, with depth-integrated axial deviatoric stresses in the ice in order to maintain force balance (cf. Shumskiy & Krass 1976; Morland 1987).

To model the ice shelf, the calving velocity v_c must be specified explicitly. In the present paper, our interest is however entirely in the grounded part of the ice sheet, and it turns out that we can exclude the ice shelf completely from consideration. The idea behind this is based on a simple consideration of force balance and of incipient flotation (cf. MacAyeal & Barcilon 1988). First, note that continuity in h at the grounding line combined with the inequality constraints (2.1) requires that h is at flotation at the grounding line, $h = (\rho_w/\rho)b$. Secondly, provided an ice shelf does exist, we can integrate the (2.2*a*) from x_c to x_g and use the second boundary condition in (2.2) as well as continuity in u_x to find

$$\left.\begin{array}{r} h = (\rho_w/\rho)b, \\ 2A^{-1/n}h|u_x|^{1/n-1}u_x = \tfrac{1}{2}(1 - \rho/\rho_w)\rho g h^2 \end{array}\right\} \text{ at } x = x_g. \qquad (2.6a, b)$$

The boundary condition in (2.6*a*) is the obvious flotation condition. Equation (2.6*b*) is a statement of horizontal force balance in the ice shelf: because the ice shelf is buoyant in sea water, it has a tendency to spread out and thin, in much the same way as a drop of oil tends to spread out on water. However, by contrast with that for an unconfined drop of oil, the spreading of the shelf is unidirectional, that is, away from the grounded shelf. In order to maintain force balance, the gravitational force driving this spreading motion must then be balanced by a non-zero axial deviatoric stress at the grounding line, as required by (2.6).

As an important aside, we note that the integration of (2.6) to yield a stress boundary condition at the grounding line is possible here only because the problem is spatially one-dimensional (in the sense that there is a single independent spatial variable, x; the shelf is obviously physically two-dimensional). For more complicated, three-dimensional, ice-shelf geometries (giving rise to a two-dimensional depth-integrated model), the axial deviatoric stress at the grounding will in general differ from that in (2.6) and must be found by solving a two-dimensional analogue of (2.2) (e.g. MacAyeal 1987; Schoof 2006*a*).

Given the integration of the force balance in the shelf, which gives rise to (2.6), we can now reduce the model for the grounded part of the ice sheet to (2.1), (2.3) and (2.6). We may also note that neither condition in (2.6) makes use of velocity continuity at x_g. This additional jump condition does not affect the flow of the grounded sheet, but provides an upstream boundary condition on the velocity field in the shelf.

Mathematically, the boundary conditions above may be interpreted as follows. Equations (2.6*b*) and (2.3*b*) serve as boundary conditions for (2.1*a*), which for fixed time t is second-order elliptic in u. The first equation in (2.3*a*) is an upstream boundary condition for the advection-type problem represented by (2.1*b*). More accurately, a consideration of characteristics shows that the system of partial differential equations (2.1) is of mixed parabolic–hyperbolic type and requires one boundary condition on each boundary for the parabolic part and initial conditions as well as an upstream boundary condition for the hyperbolic part. The additional condition given by (2.6*a*) then serves to determine the evolution of the free boundary $x_g(t)$.

In §1, we stated that a parabolic equation is typically used to describe the evolution of the ice-sheet surface. In the present model, a diffusion equation for h is obtained if the axial deviatoric stresses represented by the first term in the first (force-balance) equation in (2.1) are small. Importantly, however, the boundary condition (2.6)

imposes a fixed value on this axial deviatoric stress, which suggests that this stress may not be small at the grounding line. To explore the consequences of this observation systematically, first of all we scale the model.

2.1. *Non-dimensionalization*

Suppose we know typical scales for the horizontal extent $[x]$ of the ice sheet (given for instance by the size of the continental shelf supporting the ice sheet or by the distance over which a changes from accumulation to ablation) and the accumulation rate $[a]$. We can then define scales $[u]$, $[h]$ and $[t]$ for velocity, ice thickness and time by writing

$$C[u]^m = \rho g[h]^2/[x], \qquad [u][h]/[x] = [a], \qquad [t] = [x]/[u]. \qquad (2.7)$$

These yield the single dimensionless parameter

$$\varepsilon = \frac{A^{-1/n}([u]/[x])^{1/n}}{2\rho g[h]}. \qquad (2.8)$$

Physically, ε represents the ratio of the axial deviatoric stress and the hydrostatic pressure in the ice sheet and depends crucially on how large $[u]$ is: very fast sliding tends to correspond to larger ε.

In order to clarify the conditions under which our depth-integrated model is valid in the first place, we can also define a scale $[u_s]$ for the velocity difference between bed and ice surface caused by shearing across the thickness of the ice by writing

$$A^{-1/n}([u_s]/[h])^{1/n} = \rho g[h]^2/[x]. \qquad (2.9)$$

As will be demonstrated in the companion paper, the model (2.1)–(2.6) is then valid at leading order in the slip ratio $[u_s]/[u]$, provided that $[u_s]/[u] \ll 1$ and $[h]/[x] \ll 1$, which we assume to be the case.

Using the scales above, the model can then be scaled in the obvious way by defining $u = [u]u^*$, $h = [h]h^*$, $b = [h]b^*$, etc. We drop the asterisks immediately, and further introduce the material parameter

$$\delta = 1 - \rho/\rho_w. \qquad (2.10)$$

This allows us to define a dimensionless flotation thickness h_f through

$$h_f(x) = \frac{b(x)}{1 - \delta}. \qquad (2.11)$$

We then have the dimensionless model

$$\left.\begin{array}{r} 4\varepsilon\left(h|u_x|^{1/n-1}u_x\right)_x - |u|^{m-1}u - h(h-b)_x = 0 \\ h_t + (uh)_x = a \\ h \geqslant h_f \end{array}\right\} \text{ on } x \in (0, x_g(t)), \qquad (2.12a\text{–}c)$$

$$\left.\begin{array}{r} (h-b)_x = 0, \\ u = 0 \end{array}\right\} \text{ at } x = 0, \qquad (2.13a, b)$$

$$\left.\begin{array}{r} h = h_f, \\ |u_x|^{1/n-1}u_x = \delta h_f/(8\varepsilon) \end{array}\right\} \text{ at } x = x_g(t), \qquad (2.14a, b)$$

with initial conditions $h(x, 0) = h_0(x)$ for $x \in (0, x_g(0))$, where $x_g(0)$ is given.

From (2.12), we see that the value of ε determines whether the ice sheet is essentially a viscous jet ($\varepsilon = O(1)$) or a lubrication flow ($\varepsilon \ll 1$). In this paper, we assume the

latter, so $\varepsilon \ll 1$. This is typically true of ice sheets and can be verified using some simple scale estimates. With $[a] = 0.1 \text{ m a}^{-1}$ (1 a = 1 year = 3×10^7 s), $[h] = 1000 \text{ m}$ and $[x] = 10^6 \text{ m}$ and using $n = 3$ and $A = 6 \times 10^{-24} \text{ Pa}^{-3} \text{ s}^{-1}$ (Paterson 1994, chap. 5), we find $\varepsilon = 4 \times 10^{-4}$. The subsequent discussion will be concerned with the boundary-layer structure engendered in the mathematical problem defined by (2.12)–(2.14) when $\varepsilon \ll 1$.

3. Matched asymptotics

In the following, we will be concerned with the case $\varepsilon \ll 1$, while we treat δ as an $O(1)$ parameter: with $\rho = 900 \text{ kg m}^{-3}$, $\rho_w = 1000 \text{ kg m}^{-3}$, we have $\delta = 0.1$, while $\varepsilon \approx 10^{-4}$ as previously estimated. Ignoring the $O(\varepsilon)$ term in (2.12), we have the straightforward leading-order outer problem

$$\left. \begin{array}{r} |u|^{m-1}u = -h(h - b)_x \\ h_t + (uh)_x = a \end{array} \right\} \text{ on } x \in (0, x_g). \quad (3.1)$$

This yields for the ice velocity

$$u = -h^{1/m}|(h - b)_x|^{1/m-1}(h - b)_x \quad (3.2)$$

and allows the evolution equation in (3.1) to be rewritten as the simple diffusion equation

$$h_t - \left[h^{1+1/m}|(h - b)_x|^{1/m-1}(h - b)_x \right]_x = a. \quad (3.3)$$

The ice flux is therefore a function of the local ice thickness and surface slope, and (3.3) is a variant of the classical lubrication or shallow-ice approximation for ice-sheet flow (see also Fowler 1982). Specifically, (3.3) is the desired nonlinear diffusion equation for ice thickness h.

Note that the prescription (3.2) for the ice velocity also satisfies the second boundary condition in (2.13) at the centre of the ice sheet, provided that h satisfies the first boundary condition in (2.13) However, putting $\varepsilon = 0$ is a singular perturbation, in the sense that it does not allow the boundary conditions (2.4) to be satisfied at the grounding line. In order to satisfy these, a boundary layer near $x = x_g$ is required. The remainder of the paper will be concerned with the analysis of this boundary layer and with the boundary conditions in the outer problem at the grounding line $x = x_g$ which arise as a result.

Naïvely, one might expect a sensible boundary-layer structure to arise when the ice thickness at the grounding line is comparable with the ice thickness inland in the grounded sheet, and this is in fact implicit in some numerical studies of marine ice-sheet dynamics (e.g. Hindmarsh & LeMeur 2001). However, as we shall demonstrate in the next section, a matching of fluxes in the interior of the ice sheet with those at the grounding line actually requires a small ice thickness at the grounding line. This leads ultimately to the boundary-layer problem analysed in § 3.3 (the reader interested primarily in the practical application of matched asymptotics to real ice sheets could proceed directly to § 3.3). An analogous result was obtained previously by Wilchinsky & Chugunov (2001), who found that the ice thickness at the grounding line must be small compared with the ice thickness in the interior of the sheet.

3.1. *Thick ice at the grounding line*

In this section, we shall suppose that $h_f = O(1)$, i.e. the ice thickness at the grounding line is comparable to the ice thickness inland. We rescale near the grounding line as

follows:

$$\left.\begin{aligned}
h(x, t) &= H(X, t), \\
u(x, t) &= \varepsilon^{\alpha} U(X, t), \\
x_g - x &= \varepsilon^{\beta} X.
\end{aligned}\right\} \tag{3.4}$$

Note that x_g in the definition of X depends on t, so the time derivative h_t becomes

$$h_t = H_t + \varepsilon^{-\beta} \dot{x}_g H_X, \tag{3.5}$$

where the dot on $\dot{x}_g$ denotes an ordinary time derivative and the subscript X again indicates a partial derivative. With the rescaled variables above, (2.12a) and (2.14b) become

$$4\varepsilon^{[n+\alpha-\beta(n+1)]/n} \left(H|U_X|^{1/n-1}U_X\right)_X - \varepsilon^{\alpha m}|U|^{m-1}U + \varepsilon^{-\beta}HH_X + Hb_x = 0, \tag{3.6}$$

$$\varepsilon^{[n+\alpha-\beta]/n}|U_X|^{1/n-1}U_X = -\delta h_f/8 \qquad \text{at } X = 0, \tag{3.7}$$

where we assume that the prescribed bed slope is such that $b_x = O(1)$ and we retain b_x as the relevant bed slope (i.e. we assume that significant variations in sea-floor geometry occur only on the length scale $[x]$ associated with the width of the ice sheet). The obvious rescaling is then given by balancing the viscous and friction terms in (3.6) and by balancing terms on both sides of (3.7). This leads to the choices

$$\alpha = -\frac{n}{m+1}, \qquad \beta = \frac{mn}{m+1}, \tag{3.8}$$

which have the expected feature that $\alpha < 0$ (corresponding to large ice velocities at the grounding line compared with those inland) and $\beta > 0$ (corresponding to a boundary layer of small horizontal extent compared with the size of the ice sheet). Equations (2.12) and (2.14) then become

$$4\left(H|U_X|^{1/(n-1)}U_X\right) - |U|^{m-1}U + HH_X + \varepsilon^{mn/(m+1)}Hb_x = 0, \tag{3.9}$$

$$\varepsilon^n H_t + \varepsilon^{n/(m+1)}\dot{x}_g H_X - (UH)_X = \varepsilon^n a, \tag{3.10}$$

$$H(X, T) \geqslant h_f(x_g - \varepsilon^{mn/(m+1)}X), \tag{3.11}$$

for $X \in (0, \varepsilon^{-mn/(m+1)}x_g)$, with

$$H = h_f(x_g),$$
$$|U_X|^{1/n-1}U_X = -\delta h_f/8, \tag{3.12}$$

at $X = 0$. (Note that $(x_g - \varepsilon^{mn/(m+1)}X)$ in (3.11) is the argument of h_f, not a factor.)

At leading order,

$$\left.\begin{aligned}
4\left(H|U_X|^{1/n-1}U_X\right) - |U|^{m-1}U + HH_X &= 0 \\
(UH)_X &= 0 \\
H &\geqslant h_f
\end{aligned}\right\} \text{ on } X \in (0, \infty), \tag{3.13a–c}$$

$$\left.\begin{aligned}
|U_X|^{1/n-1}U_X &= -\delta h_f/8 \\
H &= h_f
\end{aligned}\right\} \text{ at } X = 0, \tag{3.14a, b}$$

where $h_f = h_f(x_g)$ is constant at leading order in the boundary layer.

Matching the inner and outer solutions requires that

$$\left.\begin{aligned}
h &\sim H, \\
u &\sim \varepsilon^{-n/(m+1)}U
\end{aligned}\right\} \text{ as } x \to x_g^-, \ X \to \infty, \tag{3.15a, b}$$

where the limits in x and X naturally imply limits taken in a matching region for which $1 \ll X \ll \varepsilon^{-mn/(m+1)}$, $\varepsilon^{nm/(m+1)} \ll x_g - x \ll 1$. From (3.15), we require at leading order that $U \to 0$ while H remains finite as $X \to \infty$. Since UH is constant for $X > 0$ from (3.13b), with $H \geqslant h_f > 0$, this is only possible if $U \equiv 0$. Then, however, we have a contradiction with (3.14a). Physically, the large axial deviatoric stress imposed on the grounded ice at the grounding line demands a large ice velocity, which cannot be supplied by the region upstream of the grounding line if ice thicknesses there are comparable with the ice thickness at the grounding line itself.

The only way in which the inner problem can be successfully matched with the outer problem is to also rescale the time t, by writing

$$t = \varepsilon^{n/(m+1)}T, \tag{3.16}$$

where the time scale associated with T is fast compared with that associated with the original outer time variable t. The only change in the leading-order inner problem is that the second term in (3.10) now features, so (3.13b) is replaced by

$$[(U - x'_g)H]_X = 0. \tag{3.17}$$

The prime here denotes an ordinary derivative with respect to T. While (3.13b) requires a constant flux in the boundary layer with respect to a fixed frame of reference, (3.17) now demands constant flux in a frame travelling at the velocity of the grounding line. This change allows matching with the outer solution. Specifically, let

$$H_\infty = \lim_{x \to x_g^-(T)} h(x, T) = \lim_{X \to \infty} H(X, T). \tag{3.18}$$

It follows from (3.17) and the matching conditions (3.15) that

$$(U - x'_g)H = -x'_g H_\infty = Q_\infty \qquad \text{for } X > 0, \tag{3.19}$$

and $\lim_{X \to \infty} U = 0$ no longer implies that $U \equiv 0$. Physically, the quantity Q_∞ defined in (3.19) can be identified as the rate at which the ice sheet loses mass through the grounding line. In what follows, it also represents a convenient mathematical proxy for H_∞ when x'_g is given.

Using $H = Q_\infty/(U - x'_g)$ and $HH_X = (H^2)_X/2$, the (3.13a) can be rewritten as a second-order ordinary differential equation in X:

$$4 \left(\frac{Q_\infty}{U - x'_g} |U_X|^{1/n-1} U_X \right)_X - |U|^{m-1}U + \frac{1}{2} \left(\frac{Q_\infty^2}{(U - x'_g)^2} \right)_X = 0, \tag{3.20}$$

with 'initial' conditions

$$|U_X|^{1/n-1}U_X = -\frac{\delta h_f}{8}, \qquad \frac{Q_\infty}{U - x'_g} = h_f, \tag{3.21a, b}$$

at $X = 0$. In addition, we require the solution to match with the outer problem, so that

$$U \to 0 \qquad \text{as} \qquad X \to \infty. \tag{3.22}$$

Equation (3.20) combined with (3.21a, b) and (3.22) essentially constitute a nonlinear degenerate eigenvalue problem with Q_∞ as the eigenvalue. For a given set of initial conditions (3.21), (3.20) can be solved to give U as a function of X, but in general this solution may not satisfy the matching condition (3.22). We anticipate that for fixed values of the parameters x'_g and h_f appearing in (3.20) and (3.21), successful matching is only possible for specific values of $Q_\infty = -x'_g H_\infty$.
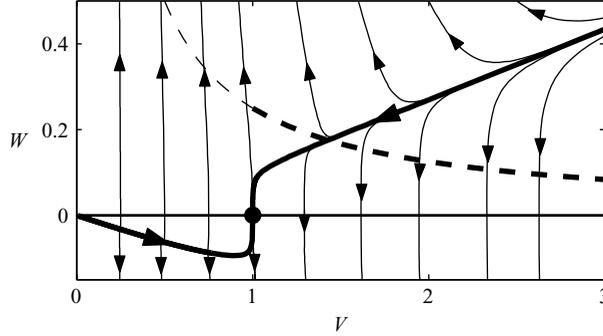
FIGURE 2. Phase plane for the system (3.24), with $\delta = 0.1$, $n = 3$, $m = 1/3$, $Q_\infty = 20$, $x'_g = -1$. Phase-trajectory directions are indicated by arrows, and separatrices approaching $(-x'_g, 0)$ at large X are shown as heavy solid lines. The hyperbola $W = \delta Q/(8H_f)$ is plotted as a dashed line, heavy in the 'allowed' domain $V > -x'_g$.

In order to analyse this problem, observe that (3.20) can be rewritten as a pair of autonomous coupled first-order ordinary differential equations. We introduce

$$V = U - x'_g, \qquad W = -|U_X|^{1/n-1} U_X. \qquad (3.23)$$

Then

$$\left.\begin{aligned} V_X &= -|W|^{n-1}W, \\ W_X &= \frac{Q_\infty |W|^{n-1}W}{4V^2} - \frac{V|V + x'_g|^{m-1}(V + x'_g)}{4Q_\infty} - \frac{|W|^{n+1}}{V} \end{aligned}\right\} \text{ on } X \in (0, \infty), \quad (3.24)$$

$$W = \frac{\delta h_f}{8}, \qquad V = \frac{Q_\infty}{h_f} \qquad \text{at } X = 0, \qquad (3.25)$$

$$\left.\begin{aligned} V &\to -x'_g \\ W &\to 0 \end{aligned}\right\} \text{ as } X \to \infty. \qquad (3.26)$$

To proceed further, take x'_g and Q_∞ to be fixed. Since $H_\infty = Q_\infty/(-x'_g) > 0$, there are then two scenarios to consider: either $Q_\infty > 0$, $x'_g < 0$ or vice versa. From (3.21b), we can identify these cases with those of positive and negative ice velocities at the grounding line, respectively; we have $x'_g = -h_f U(0)/(H_\infty - h_f)$ and, with $H_\infty > h_f > 0$, x'_g is opposite in sign to the velocity $U(0)$ at the grounding line. (Incidentally, $x'_g = -h_f U(0)/(H_\infty - h_f)$ takes the form of a Rankine–Hugoniot condition: because $U(\infty) = 0$, $x'_g = -h_f U(0)/(H_\infty - h_f) = [H_\infty U(\infty) - h_f U(0)]/[H_\infty - h_f] = [HU]_0^\infty/[H]_0^\infty$ in an obvious notation.)

Regardless of whether x'_g is positive or negative, the point $(-x'_g, 0)$ in the (V, W)-plane is a degenerate saddle, as shown in the phase portraits in figures 2 and 3. In each case, there are precisely two trajectories (or *separatrices*) approaching $(-x'_g, 0)$ for large X, one from above the V-axis and one from below (plotted as heavy solid lines in figure 2). In addition, there are two further trajectories which emerge from $(-x'_g, 0)$ in such a way that $(V, W) \to (-x'_g, 0)$ for $X \to -\infty$ (and which are therefore of no concern here). In order to satisfy the matching condition (3.26), the solution of (3.24)–(3.26) must therefore follow one of the two separatrices which approach the saddle point for large X.
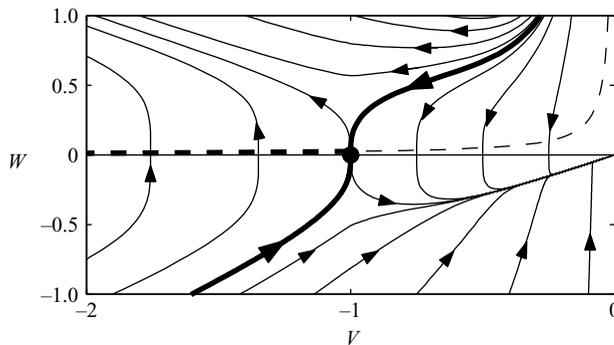
FIGURE 3. Same as figure 2, but with $\delta = 0.1$, $n = 3$, $m = 1/3$, $Q_\infty = -1$, $x'_g = 1$. The hyperbola $W = \delta Q/(8H_f)$ is again shown as a dashed line, the 'allowed' domain now being $V < -x'_g$. The heavy dashed line does not intersect either of the phase paths (drawn as heavy solid lines), which approach $(-x'_g, 0)$ for large X.

The behaviour of these separatrices near the saddle point can be determined explicitly. From (3.24), phase paths satisfy

$$\frac{\mathrm{d}W}{\mathrm{d}V} = -\frac{Q_\infty}{4V^2} + \frac{V|V + x'_g|^{m-1}(V + x'_g)}{4Q_\infty|W|^{n-1}W} + \frac{W}{V}. \tag{3.27}$$

The local form of the separatrices close to the saddle point $(-x'_g, 0)$ can be found by looking for solutions of the form $V = -x'_g + v$, $W = C|v|^{\nu-1}v$ for small v, where the constants C and $\nu > 0$ are to be determined. Assuming $m < n$, which is typically the case, we find that

$$W \sim \left(\frac{(n+1)|-x'_g|}{4Q_\infty(m+1)}\right)^{1/(n+1)} |V + x'_g|^{(m+1)/(n+1)-1}(V + x'_g) \tag{3.28}$$

for separatrices approaching the saddle point. The observation that will become important in what follows is this: from (3.28), it is clear that the separatrix which lies above the V-axis corresponds to $V > -x'_g$, while the separatrix below the V-axis has $V < -x'_g$. As the phase portraits in figures 2 and 3 show, this appears to be true globally, and not just close to the saddle point. Furthermore, it is clear that the shape of the separatrices can depend only on the parameters m, n, δ, Q_∞ and x'_g appearing in (3.24)–(3.26).

It remains to impose the initial conditions (3.25), which requires us to distinguish between the different possible signs for Q_∞. We consider first the physically more intuitive case $Q_\infty > 0$, $x'_g < 0$, corresponding to mass loss from the ice sheet at the grounding line. This is illustrated in figure 2. In order to satisfy the initial condition, the point $(Q_\infty/h_f, \delta h_f/8)$ must lie on one of the separatrices. Since $\delta h_f/8 > 0$ for $h_f > 0$, this must be the separatrix above the V-axis. If we keep Q_∞ fixed while h_f varies, the locus of points $(Q_\infty/h_f, \delta h_f/8)$ traces a hyperbola of the form $W = \delta Q_\infty/(8V)$ in the (V, W)-plane, and the point of intersection between the separatrix and the hyperbola defines the point corresponding to the appropriate initial conditions. However, as we require $h_f \leqslant H_\infty = Q_\infty/(-x'_g)$ and $V = Q_\infty/h_f$, only that part of the hyperbola which lies to the right-hand side of $V = -x'_g$ is of interest (plotted as a heavy broken line in figure 2). For the case $Q_\infty > 0$, there is clearly a single point of intersection between the 'allowed' part of the hyperbola and the separatrix, and the W-coordinate W_f of
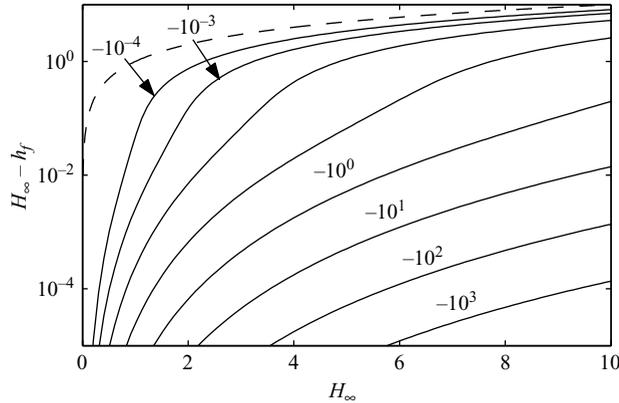
FIGURE 4. Contour plots of $x'_g = -v_g$ against H_∞ and $H_\infty - h_f$. Note the logarithmic scale on the vertical axis. The solid-line contour levels are also spaced logarithmically from -10^{-3} (bottom right) to -10^{-4} (top left). The dashed line is $H_\infty - h_f = H_\infty$, and indicates the boundary of the domain of x'_g as we must have $h_f > 0$ (there is another domain boundary at $H_\infty - h_f = 0$, as we must also have $H_\infty > h_f$).

that point gives us the unique value $h_f = 8W_f/\delta$, which corresponds to the given Q_∞, x'_g, m, n and δ.

We can repeat this procedure for $Q_\infty < 0$, corresponding to the case where ice flows into the grounded ice sheet from beyond the grounding line. Again, we have to look for points of intersection between the hyperbola given by $(Q_\infty/h_f, \delta h_f/8)$ and the separatrix emerging from $(-x'_g, 0)$ into the upper half-plane. The inequality $h_f \leqslant H_\infty = Q_\infty/(-x'_g)$ now constrains us to that part of the hyperbola $W = \delta Q_\infty/(8V)$ which lies to the left of $V = -x'_g$. However, the separatrix above the V-axis lies to the right of $V = -x'_g$. Consequently, the allowed part of the hyperbola does not intersect the separatrix, as also indicated in figure 3. There are no physically acceptable solutions for which there is a grounding line advance, and ice must flow out of the grounded ice sheet through the grounding line, as may be expected intuitively.

For $x'_g < 0$ and given material parameters m, n and δ, the boundary-layer problem therefore furnishes a relationship between h_f, $Q_\infty = -x'_g H_\infty$ and x'_g, which in general can only be evaluated numerically. As we shall see shortly, what we require in the outer problem is this relationship in the form

$$x'_g = -v_g(H_\infty, h_f), \qquad (3.29)$$

giving the rate of grounding-line migration as a function of the parameters H_∞ and h_f. In figure 4 we present contour plots of x'_g for a particular set of parameter values. These plots illustrate that v_g is clearly a single-valued function which increases with both H_∞ and h_f (as, for a given H_∞, contour levels decrease with $H_\infty - h_f$).

3.2. *Thick ice at the grounding line: the outer problem*

Next, we consider the outer problem corresponding to the boundary-layer description in §3.1. Recall that a rescaling in time to a fast time variable $T = \varepsilon^{-n/(m+1)}t$ was required in order to match the large fluxes in the boundary layer with the outer problem. When we rescale the outer problem (3.3) accordingly, we obtain

$$h_T - \varepsilon^{n/(m+1)} \left[h^{1+1/m} |(h-b)_x|^{1/m-1} (h-b)_x \right]_x = \varepsilon^{n/(m+1)} a, \qquad (3.30)$$

where the subscript T again denotes a partial derivative. At leading order, we therefore have the uninspiring statement

$$h_T = 0. \tag{3.31}$$

Owing to the fast time scale imposed by the inner problem, the ice-sheet profile is stagnant at leading order and we simply have $h(x, T) = h_0(x)$, as given by the initial condition. The only evolving quantity in the outer problem is therefore the grounding line x_g, whose motion is given by (3.29). The right-hand side of (3.29) contains the arguments H_∞ and h_f. From (3.18), it is straightforward to identify $H_\infty = h_0(x_g(T))$ as the initial ice thickness at position x_g, while $h_f = h_f(x_g(T))$ is given by the shape of the sea floor there, through (2.11). In general, H_∞ and h_f will differ, owing to an $O(1)$ change in ice thickness across the boundary layer.

Physically, the outer problem describes the rapid disintegration of the ice sheet (on the T time scale) through mass loss at the grounding line. This interpretation is borne out by numerical solutions of the original problem (2.12)–(2.14) with sufficiently large h_f (see figure 8). Of course, the outer problem above is physically nonsensical as there is no reason why such an ice sheet should exist in the first place. In other words, a marine ice sheet which is able to persist on its natural (t) time scale cannot have a flotation height h_f which is $O(1)$.

There is, however, a natural remedy for this. In the outer problem above, the rate of grounding-line retreat tends to zero as h_f does (see figure 3). Thus, for small h_f, the outer problem above predicts an essentially completely stagnant ice sheet on the fast T time scale, which suggests that a rescaling in time is again required, depending on how small h_f is. In addition, small h_f values also suggest a rescaling in h (and hence u) near the grounding line from the case considered above, and this in turn affects the matching with the outer flow. Below, we consider the case of a grounding-line thickness h_f which is small enough that the natural time scale recovered is the original t time scale, which also implies that grounding-line migration and the evolution of the ice sheet outside the boundary layer occur on the same time scale (so we no longer have the rapid retreat of the grounding line into a stagnant ice sheet).

3.3. *Small ice thickness at the grounding line*

As we have seen, the main problem in trying to force h_f to be $O(1)$ is that this implies large ice fluxes at the grounding line, which accounts for the rapid retreat of the grounding line. Below, we consider a distinguished limit which corresponds to $O(1)$ ice fluxes at the grounding-line as well as to small ice thicknesses there, so that the marine ice sheet must be located in a relatively shallow ocean. Specifically, we put $h_f = \varepsilon^\gamma H_f$ for an appropriately chosen $\gamma > 0$ (which dictates how thin the ice at the grounding line must be for a given ε) and suppose that $H_f = O(1)$ in the asymptotic limit $\varepsilon \to 0$. We emphasize that, as before, the (scaled) flotation thickness $H_f(x)$ depends on position, as a result of the varying depths of the sea floor below sea level. We merely assume that these depths are small compared with the natural thickness scale of the ice sheet.

We rescale near the grounding line as follows:

$$\left. \begin{array}{l} h(x, t) = \varepsilon^\gamma H(X, t), \\ u(x, t) = \varepsilon^\alpha U(X, t), \\ x_g - x = \varepsilon^\beta X, \end{array} \right\} \tag{3.32}$$

where α and β may be different from their values in §3.1 and $\gamma = -\alpha$, so that the rescaled flux $\varepsilon^{\alpha+\gamma} U H$ in the boundary layer remains $O(1)$. In addition, we also recognize that if the flotation thickness $h_f \sim \varepsilon^\gamma$ then the depth to the sea floor,

$b = (1-\delta)h_f$, must also be small, with $b \sim \varepsilon^\gamma$. Hence we rescale $b(x) = \varepsilon^\gamma B(x)$. However, we also assume that the rescaled depth to sea floor B only varies significantly on the outer length scale associated with the original spatial variable x and retain B_x as the relevant derivative when we rescale (2.12a–c), based on the assumption that $B_x = O(1)$.

The rescaled versions of (2.12) and of the second equality in (2.14) are then

$$4\varepsilon^{1+\alpha/n-\beta/n}\varepsilon^{\gamma-\beta}\left(H|U_X|^{1/n-1}U_X\right)_X - \varepsilon^{\alpha m}|U|^{m-1}U + \varepsilon^{2\gamma-\beta}HH_X + \varepsilon^{2\gamma}HB_x = 0, \quad (3.33)$$

$$4\varepsilon^{1+\alpha/n-\beta/n}|U_X|^{1/n-1}U_X = -\delta\varepsilon^\gamma H_f/8 \qquad \text{at } X = 0. \quad (3.34)$$

The required rescaling must balance the first two terms in (3.33), in order to describe the decay of the axial deviatoric stress over the boundary layer, and both sides of (3.34) in order to allow the boundary conditions at the grounding line to be satisfied. Equating the relevant exponents of ε in (3.33), (3.34) and enforcing $\alpha = -\gamma$ yields the distinguished limit

$$\alpha = -\frac{n}{n+m+3}, \qquad \beta = \frac{n(m+2)}{n+m+3}, \qquad \gamma = \frac{n}{n+m+3}. \quad (3.35)$$

With these choices of α, β and γ, the scaled problem becomes

$$4\left(H|U_X|^{1/(n-1)}U_X\right) - |U|^{m-1}U + HH_X - \varepsilon^{n(m+2)/(n+m+3)}HB_x = 0, \quad (3.36)$$

$$\varepsilon^{n(m+3)/(n+m+3)}H_t + \varepsilon^{n/(n+m+3)}\dot{x}_g H_X - (UH)_X = \varepsilon^{n(m+2)/(n+m+3)}a \quad (3.37)$$

for $X \in (0, \varepsilon^{-n(m+2)/(n+m+3)}x_g)$, with

$$\left.\begin{array}{l} H = H_f, \\ |U_X|^{1/n-1}U_X = -\delta H_f/8, \end{array}\right\} \quad (3.38)$$

at $X = 0$.

Ignoring higher-order terms in ε, the boundary-layer problem becomes

$$\left.\begin{array}{r} 4\left(H|U_X|^{1/n-1}U_X\right) - |U|^{m-1}U + HH_X = 0 \\ (UH)_X = 0 \\ H \geqslant H_f \end{array}\right\} \text{ on } X \in (0, \infty) \quad (3.39a\text{--}c)$$

$$\left.\begin{array}{l} H = H_f \\ |U_X|^{1/n-1}U_X = -\delta H_f/8 \end{array}\right\} \text{ at } X = 0, \quad (3.40)$$

where $H_f = H_f(x_g)$ is again constant at leading order. Matching with the outer solution now requires that

$$\left.\begin{array}{l} uh \sim UH, \\ u \sim \varepsilon^{-n/(n+m+3)}U \\ h \sim \varepsilon^{n/(n+m+3)}H \end{array}\right\} \text{ as } x \to x_g^-(t), \; X \to \infty. \quad (3.41)$$

By analogy with (3.13b) and (3.15b), the inner solution has $U \to 0$ while $UH = Q$ remains constant on account of (3.39). Following the same argument as before, it is clear that $Q \neq 0$ since $Q = 0$ does not allow the second equality in (3.40) to be satisfied. However, by contrast with §3.1, this no longer presents a problem as the matching conditions (3.41) allow for H to diverge as $X \to \infty$.
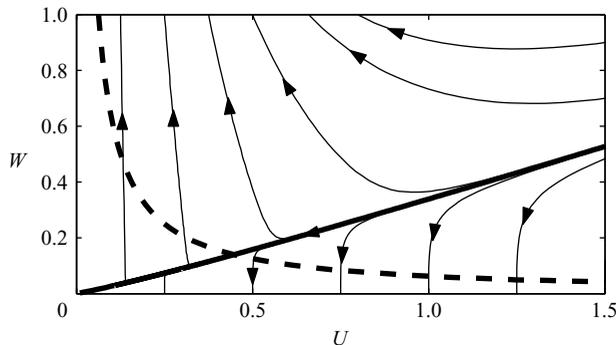
FIGURE 5. Phase plane for the system (3.46), with $\delta = 0.1$, $n = 3$, $m = 1/3$, $Q = 5$. Phase path directions are indicated with arrows, and the separatrix approaching the origin from the first quadrant at large X is shown as a heavy solid line. The hyperbola $W = \delta Q/(8U)$ is shown as a dashed line.

Again, we exploit $H = Q/U$ to rewrite (3.39a) as a nonlinear ordinary second-order differential equation analogous to (3.20):

$$4\left(\frac{Q}{U}|U_X|^{1/n-1}U_X\right)_X - |U|^{m-1}U + \frac{1}{2}\left(\frac{Q^2}{U^2}\right)_X = 0 \qquad \text{on } X \in (0, \infty), \qquad (3.42)$$

subject to 'initial' conditions

$$|U_X|^{1/n-1}U_X = -\delta H_f/8, \qquad U = Q/H_f, \qquad \text{at } X = 0, \qquad (3.43)$$

and with

$$U \to 0 \qquad \text{as } X \to \infty. \qquad (3.44)$$

The resulting eigenvalue problem for Q is analogous to that for Q_∞ in §3.1. Again, we can shift to a phase plane by defining

$$W = -|U_X|^{1/n-1}U_X. \qquad (3.45)$$

Then

$$\left.\begin{array}{rcl} U_X & = & -|W|^{n-1}W \\[1mm] W_X & = & \dfrac{Q|W|^{n-1}W}{4U^2} - \dfrac{|U|^{m+1}}{4Q} - \dfrac{|W|^{n+1}}{U} \end{array}\right\} \text{ on } X \in (0, \infty), \qquad (3.46)$$

$$\left.\begin{array}{l} U = Q/H_f \\[1mm] W = \delta H_f/8 \end{array}\right\} \text{ at } X = 0 \qquad (3.47)$$

$$(U, W) \to (0, 0) \text{ as } X \to \infty. \qquad (3.48)$$

As we shall show in the next section, we must have a non-negative flux Q, which therefore leaves $Q > 0$ as $Q \neq 0$. Moreover, from the inequality in (3.39), $H(X, t) \geqslant H_f > 0$ for all $X > 0$. Hence it follows that $U > 0$ throughout the boundary layer. Since $U \to 0$ for large X, (U, W) must therefore follow a trajectory which approaches the origin from the first quadrant of the (U, W)-plane. As before, the origin is a degenerate saddle and, as shown in the phase portrait in figure 5, there is a unique trajectory such that $(U, W) \to 0$ from the first quadrant as $X \to \infty$. The shape of this trajectory depends only on the parameters Q, m, n and δ appearing in (3.46) and (3.47) and, as before, one can look for a local form $W \sim CU^\nu$ wih W, U small.
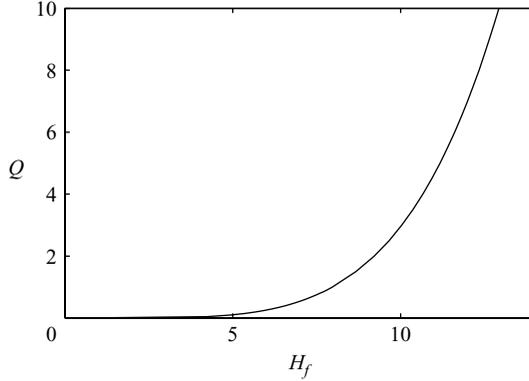
FIGURE 6. Grounding-line flux Q as a function of the scaled grounding-line thickness H_f for $n = 3$, $m = 1/3$, $\delta = 0.1$. For the range of values of H_f shown, Q is within a fractional error of less than 10^{-3} of the asymptotic form (3.51).

This yields

$$W \sim \frac{U^{(m+3)/n}}{Q^{2/n}}. \tag{3.49}$$

In order also to satisfy the initial conditions (3.43), we see that the point $(Q/H_f, \delta H_f/8)$ must again lie on the separatrix. When Q is kept constant while H_f is varied, the locus of points of the form $(Q/H_f, \delta H_f/8)$ again traces a hyperbola, as shown in figure 5. For a given flux Q, the U-coordinate U_f of the intersection of that curve with the separatrix defines the corresponding value of H_f through $H_f = Q/U_f$. As the phase plot in figure 5 strongly suggests, there appears to be a unique thickness H_f for a given Q. By analogy with the discussion in §3.1, we therefore obtain a relationship between the scaled flotation thickness H_f and the flux Q at the grounding line in the outer problem, which we write here in the form $Q = q_g(H_f)$. This relationship then serves as a boundary condition on the outer problem (3.3) at the grounding line and, as we shall see in the next section, it supplies the missing Stefan-type condition necessary to predict the evolution of the grounding line in time.

It is even possible to find the behaviour of $q_g(H_f)$ explicitly for small H_f. Using (3.49), we obtain

$$\frac{\delta H_f}{8} = \frac{(Q/H_f)^{(m+3)/n}}{Q^{2/n}}, \tag{3.50}$$

or equivalently

$$Q = (\delta/8)^{n/(m+1)} H_f^{(m+n+3)/(m+1)}. \tag{3.51}$$

It is worth pointing out that Hindmarsh (2006) has independently deduced some of the qualitative features of the boundary-layer problem above. Based on monotonicity arguments, he demonstrates that for a given grounding-line thickness h_f, only a restricted range of fluxes can be possible. The novelty here is that we are able to show that there is in fact a single flux $q_g(H_f)$ corresponding to h_f and that we furnish an explicit way of calculating $q_g(H_f)$. Moreover, the scaling for h in the boundary layer is novel in this paper, demonstrating explicitly that the ice thickness at the grounding line must be small in order to match successfully to the outer problem.

For more general H_f, q_g can only be computed numerically, and an example for a particular choice of the parameters m and n is shown in figure 6. As one

would expect, $q_g(H_f)$ is single-valued, positive and monotonically increasing in H_f for $H_f > 0$: the ice flux at the grounding line increases rather than decreases, with water depth. Notably, the numerically calculated form of q_g agrees very closely with the asymptotic form (3.51) valid for small H_f. (This can probably be explained by the fact that $\delta = 0.1$ is relatively small; as shown in Appendix A.1, (3.51) is also valid for $H_f \sim O(1)$ provided that $\delta \ll 1$). Moreover, numerically, q_g diverges as H_f tends to infinity. This is in line with the result of §3.1: for large H_f, we expect fluxes at the grounding line that are large compared with fluxes inland.

3.4. *The outer problem for a marine ice sheet: steady profiles*

Next, we turn our attention to the outer problem which corresponds to the boundary-layer problem discussed in §3.3. Recall that we set $b = \varepsilon^{n/(n+m+3)}B$ in order to account for the shallow depths of the sea floor. Rescaling (3.3) accordingly and retaining only leading-order terms, this leaves the simpler expression

$$h_t - \left(h^{1/m+1}|h_x|^{1/m-1}h_x\right)_x = a \tag{3.52}$$

for $x \in (0, x_g)$, with

$$h_x = 0, \tag{3.53}$$

at $x = 0$.

Meanwhile, the matching conditions (3.41) with $UH = Q$ yield the boundary conditions

$$h(x_g(t), t) = 0, \qquad \lim_{x \to x_g^-(t)} -h^{1/m+1}|h_x|^{1/m-1}h_x = Q, \tag{3.54a, b}$$

at $x = x_g$. In order to ensure non-negative h near x_g, it follows from these boundary conditions that we must have $h_x \leqslant 0$ and hence $Q \geqslant 0$, as previously claimed. The boundary condition in (3.54a) dispenses with the flotation condition at the grounding line in favour of zero ice thickness at leading order. This is obviously the result of having small ice thickness at the grounding line. The shape of the sea floor and hence the function h_f now enter the problem solely through the second (flux) boundary condition in (3.54). The inner problem supplies Q as a function of the scaled flotation thickness H_f through

$$Q(x_g) = q_g(H_f(x_g)) = (\delta/8)^{n/(m+1)}[H_f(x_g)]^{(m+n+3)/(m+1)}, \tag{3.55}$$

where we have assumed the asymptotic form of q_g in (3.51).

In other words, the assumed shallow shape of the ice-sheet bed affects the ice-flow problem at leading order only by prescribing a flux at the grounding line. This flux is a function of the position of the grounding line through (3.55). As in the case of a land-based ice sheet, we obtain again a degenerate diffusion equation, the degeneracy arising because the diffusion coefficient vanishes when h does. This occurs at leading order at the moving boundary $x = x_g(t)$ of the domain. The marine ice-sheet case therefore differs from the land-based one because the ice flux uh at the grounding line is non-zero, being determined instead by the prescribed (scaled) flotation thickness H_f through the function q_g in (3.55).

Next, we consider the simpler steady-state problem. Omitting time derivatives, we have

$$(uh)_x = a, \qquad u = -h^{1/m}|h_x|^{1/m-1}h_x \qquad \text{on } x \in (0, x_g), \tag{3.56}$$

$$h_x = 0 \qquad \text{at } x = 0, \tag{3.57}$$

$$h = 0, \qquad \lim_{x \to x_g^-} uh = q_g(H_f(x_g)) \qquad \text{at } x = x_g, \qquad (3.58a, b)$$

where a is independent of t. We reiterate that (3.56)–(3.58) is a free-boundary problem because the grounding-line position x_g is not known *a priori* but must be found as part of the solution.

From (3.56) and (3.57), it is straightforward to show that the flux at a position x equals the total rate of ice accumulation upstream of that point (see also Fowler 1997, chap. 18). Denoting this by $s(x)$, we have

$$u(x)h(x) = s(x) := \int_0^x a(x')\,dx'. \qquad (3.59)$$

From (3.58b) the grounding-line position x_g is therefore determined implicitly through

$$s(x_g) = \int_0^{x_g} a(x')\,dx' = q_g(H_f(x_g)). \qquad (3.60)$$

Given a solution x_g, the ice-surface profile can then be computed from

$$-h^{1/m+1}|h_x|^{1/m-1}h_x = s \qquad \text{on } x \in (0, x_g), \qquad h(x_g) = 0. \qquad (3.61)$$

Hence

$$h^{m+1}h_x = \frac{1}{m+2}(h^{m+2})_x = -|s|^{m-1}s. \qquad (3.62)$$

Together with $h(x_g) = 0$, this can be solved to give

$$h(x) = \left[(m+2)\int_x^{x_g} |s(x')|^{m-1}s(x')\,dx'\right]^{1/(m+2)}, \qquad (3.63)$$

where we also require $h \geqslant 0$ in $(0, x_g)$ as before.

The solvability of the steady ice-sheet problem thus depends on the transcendental equation (3.60) having a solution, which determines the position of the free boundary x_g. Further, the solution must be such that (3.63) predicts positive ice thicknesses (note that this is always the case provided that $s > 0$ in $(0, x_g)$).

In other words, the existence of steady ice sheet profiles depends in a non-trivial way on the accumulation rate $a(x)$ and on the shape of the sea floor, which in turn determines $H_f(x)$ (recall that $H_f = \varepsilon^{-n/(n+m+3)}b/(1 - \delta)$ is simply a scaled form of the depth b of the sea floor). Provided that solutions do exist, the corresponding grounding-line positions and surface profiles are straightforward to calculate numerically from (3.60) and (3.63).

A particular example is given in figure 7. The shape of the sea floor chosen here for illustration purposes takes the form

$$H_f(x) = 10 - 5x^2 + 5x^4/4, \qquad (3.64)$$

as shown in the centre panel of figure 7. With this choice, there is a shallow 'sill' in the sea floor around $x = 1.4$ a somewhat deeper central region around the centre of the 'continental shelf' around $x = 0$ and a sharp drop-off around $x = 2.5$.

We chose this profile to illustrate the possibility of multiple steady solutions and also because the sea floor in West Antarctica has a qualitatively similar shape, with a depression at the centre of the ice sheet and a shallower sill at the continental shelf edge. With a constant accumulation rate $a = 1$, $s(x) = ax$ on the left-hand side of (3.60) is monotonically increasing in x with $s(0) = 0$ (see figure 7c). Meanwhile, the right-hand side has $Q(0) = q_g(H_f(0)) > 0$ as $H_f(0) > 0$; $Q(x) = q_g(H_f(x))$ decreases
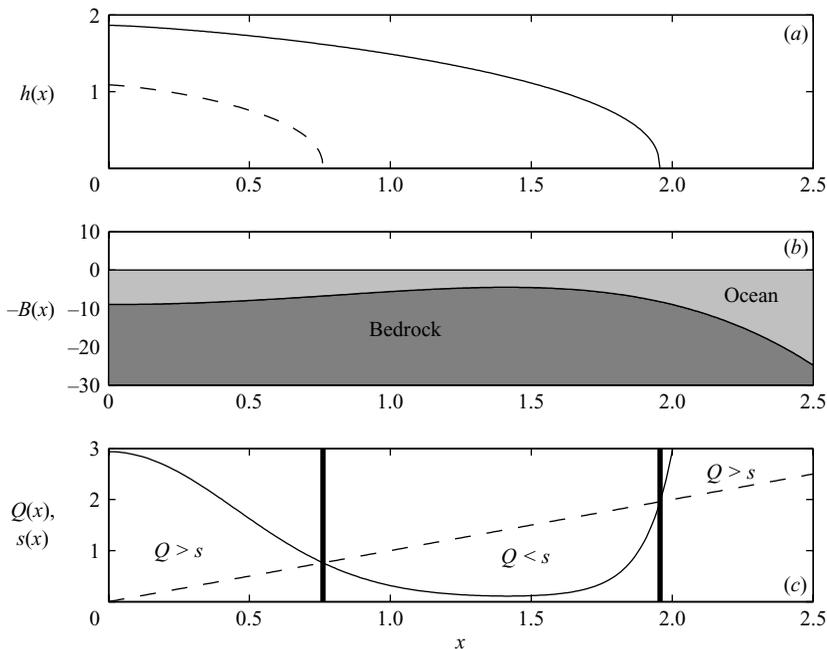
FIGURE 7. Steady ice-sheet configurations (*a*) for parameter values $\delta = 0.1$, $m = 1/3$, $n = 3$, $a = 1$, with H_f given by (3.64). (*b*) The shape of the sea floor, $-B(x) = -(1 - \delta)H_f(x)$, with bedrock shaded in dark grey and ocean shaded light grey. Steady margin positions x_g occur at points of intersection of the graphs of $s(x)$ and $Q(x) = q_g(H_f(x))$, shown in (*c*) as dashed and solid lines, respectively. The margin positions are marked by vertical solid lines. For grounding-line positions between these vertical lines we have $Q < s$, i.e. accumulation exceeds outflow and the ice sheet should grow away from the smaller steady surface profile and towards the larger one. If the conjectures leading up to (3.66) are correct then the dashed shape in (*a*) is an unstable configuration: a slightly larger ice sheet will grow while a slightly smaller one would shrink. Note that the grounding line for the dashed shape is at a position where the bed slopes upwards. The solid line in (*a*) should correspond to a stable shape.

with x to the left-hand side of the sill, where H_f decreases with x, while $H_f(x)$ and hence $Q(x) = q_g(H_f(x))$ increase with x to the right-hand side of the sill. With the particular choice of H_f above, this results in the graphs of $s(x)$ and $q_g(H_f(x))$ having two points of intersection, whose abscissae correspond to steady-state grounding-line positions x_g (figure 7*c*). Hence there are two distinct steady profiles. One of these, shown as a dashed line in figure 7(*a*), has its grounding line at $x_g = 0.7609$, which is upstream of the sill in a region where the sea floor is upward-sloping (i.e. $H_f' < 0$, as H_f measures the depth below sea level), while the other has its grounding line beyond the sill at $x_g = 1.957$, where the sea floor is downward-sloping ($H_f' > 0$).

Given multiple steady-state solutions, a relevant question is whether a given steady ice-sheet configuration is stable. This underpins the problem of marine ice-sheet instability identified by Weertman (1974).

A full linear stability analysis of steady solutions of the model (3.52)–(3.55) is beyond the scope of this paper, owing in part to the complexities introduced by the degeneracy of the problem (see also Fowler 2001; Wilchinsky 2001; Wilchinsky & Feltham 2004). Nonetheless we observe the following: as in the numerical example in figure 7, suppose that a is positive everywhere, which is relevant to cold continents such as Antarctica (but less so for ice sheets in warmer regional climates, such as

Greenland). Consider the total mass balance of the ice sheet when the grounding line is displaced slightly from its steady-state position x_g to a perturbed position $x_g + \Delta x_g$. The total rate of ice accumulation on the grounded sheet then changes to $s(x_g + \Delta x_g) = \int_0^{x_g + \Delta x_g} a(x')\,dx'$, while the rate of mass loss through the grounding line changes from $q_g(H_f(x_g)) = s(x_g) = \int_0^{x_g} a(x')\,dx'$ to $q_g(H_f(x_g + \Delta x_g))$. The net rate at which the ice sheet gains mass with its grounding line in the perturbed position is therefore

$$\int_0^{x_g + \Delta x_g} a(x')\,dx' - q_g(H_f(x_g + \Delta x_g)) \approx [a(x_g) - q_g'(H_f(x_g))H_f'(x_g)]\Delta x_g. \quad (3.65)$$

On the right-hand side we have linearized the changes in s and q_g and used the fact that $\int_0^{x_g} a(x')\,dx' - q_g(H_f(x_g)) = 0$ at the steady-state grounding-line position x_g. Heuristically, one might expect a steady profile to be stable if a small increase in ice sheet width ($\Delta x_g > 0$) leads to a decrease in net mass balance, which should cause the ice sheet to shrink back to its original size (see also Wilchinsky 2001, §4). In other words, one might expect

$$H_f'(x_g) > a(x_g)/q_g'(H_f(x_g)) \quad (3.66)$$

as a stability criterion. Since we are assuming that $a(x_g) > 0$ and that q_g is an increasing function, stability should require a sea floor which is sloping downwards sufficiently steeply at the grounding line, so that the flotation thickness H_f is a sufficiently rapidly increasing function of downstream position. If correct, this confirms Weertman's (1974) conjecture regarding marine ice-sheet instability for ice sheets with upward-sloping beds.

Graphically, steady-state margin positions x_g correspond to points of intersection between the graphs of $s(x) = \int_0^x a(x')\,dx'$ and $q_g(H_f(x))$ as functions of x (see figure 7c). According to (3.66), stable margin positions should then correspond to positions where the graph of $q_g(H_f(x_g))$ crosses that of $s(x_g)$ from below. Taking this result at face value, we expect the solution shown as a dashed line in figure 7(a) to be unstable while the solid line, whose grounding line is in a region where the sea floor is downward-sloping, should represent a stable steady state. This is of course simplistic (but notably agrees with the results of Wilchinsky 2001), and a full stability analysis remains to be done. However, the numerical results in the next section go some way to confirming our conjectures.

4. Numerical results

One of the advantages of the model (2.12)–(2.14) is that it can be solved numerically to provide validation of our asymptotic results. To deal with the moving boundary, we map first to a fixed domain $(0, 1)$ in the coordinates (σ, τ) by putting $\sigma = x/x_g$, $\tau = t$ (e.g. Crank 1984). The transformed equations are then discretized using finite differences with a staggered grid for u and h. The first equation in (2.12) is discretized using centred differences, while an upwind scheme with a backward Euler step is used for the second (evolution) equation in (2.12). The fully implicit time step also facilitates direct implementation of the flotation condition in (2.14), rather than reliance on a differentiated version which determines the rate of grounding-line migration, as is done in e.g. Vieli & Payne (2005).

In figures 8 and 9, we present results relevant to the two different boundary-layer descriptions studied in §3.1 and 3.3. Figure 8 shows a numerical solution computed for a marine ice sheet with an $O(1)$ flotation thickness. As predicted by the analysis
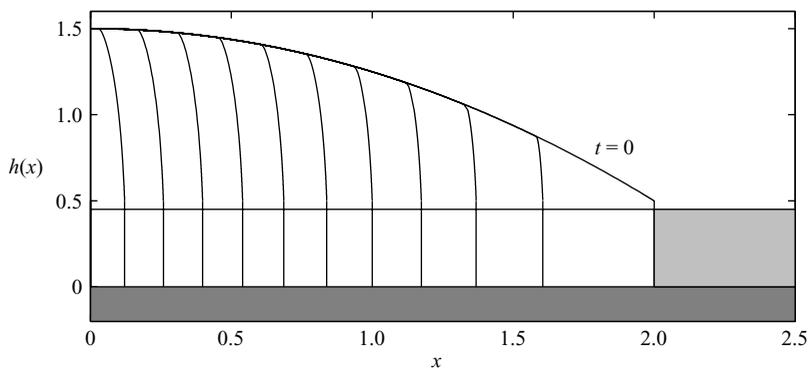
FIGURE 8. Solution of (2.12)–(2.14) showing fast grounding-line retreat for the case $h_f = O(1)$. Here $h_f = 1/2$ and $a = 1$ are independent of position. The parameter values used are $n = 3$, $m = 1/3$, $\delta = 0.1$, $\varepsilon = 5 \times 10^{-5}$. Ice sheet surface profiles are shown at time intervals of 2×10^{-5}, starting with a parabolic profile with $x_g = 2$. The upper horizontal line indicates sea level, with bedrock shaded dark grey and ocean at its minimum extent shaded light grey. Numerically, the ice sheet disappears in finite time and is almost stagnant upstream of the moving boundary layer near the grounding line.
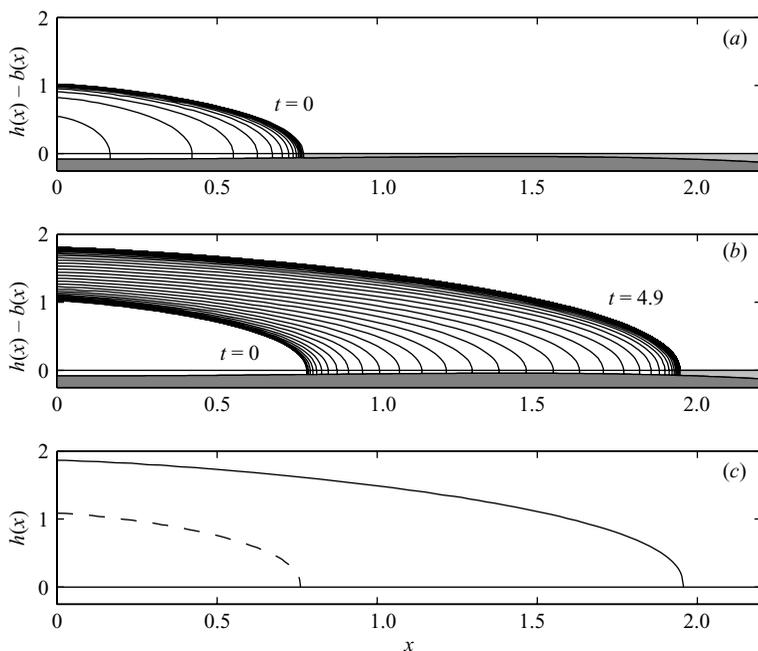

FIGURE 9. Solution of (2.12)–(2.14) with the same ice sheet bed as is assumed in figure 7. The parameter values are $n = 3$, $m = 1/3$, $\delta = 0.1$, $\varepsilon = 5 \times 10^{-5}$, while $a = 1$ and $h_f(x) = b(x)/(1 - \delta) = \varepsilon^{n/(n+m+3)}(10 - 5x^2 + 5x^4/4)$. (a, b) Ice sheet surface profiles at time intervals of 0.1, starting with initial profiles close to the dashed profile in figure 7(a). The horizontal line indicates sea level, while the bedrock is shaded dark grey and the minimum ocean extent light grey. (c) The previously calculated steady-state profiles from figure 7.

in §3.2, the ice sheet remains essentially stagnant upstream of a narrow boundary layer at the moving grounding line and rapidly loses mass through the grounding line. Numerically, the ice sheet shrinks to zero size in finite time.
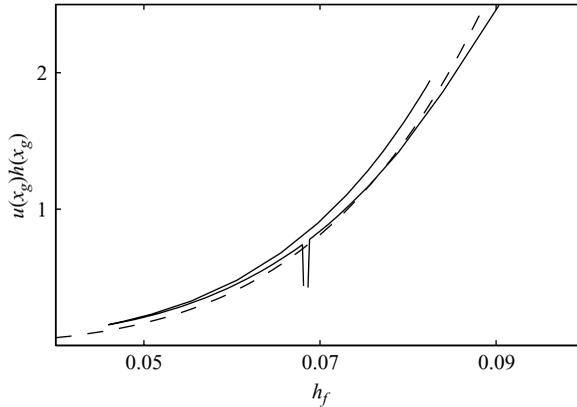
FIGURE 10. The flux $u(x_g)h(x_g)$ at the grounding line, computed as part of the numerical solutions shown in figure 9 and plotted as solid lines against $h_f(x_g)$; the corresponding flux $q_g(H_f)$ as shown in figure 6 is plotted as a broken line, with $H_f = \varepsilon^{-n/(n+m+3)}h_f$. The vertical parts of the solid lines represent a transient in which the surface profile in the boundary layer adjusts to ensure a locally constant flux. Specifically, the initial ice-surface profile in the boundary layer may not satisfy the steady boundary-layer problem in § 3.3. In this case, the ice surface in the boundary layer will relax to the shape predicted by the steady-state problem (3.39)–(3.41) over a time scale that is fast compared with the t time scale. The vertical parts of the solid lines correspond to the changes in flux that accompany this relaxation. After the transient, the solid lines agree relatively closely with the broken line.

Figure 9 shows results for the physically more relevant case of a small flotation thickness, as considered in §§ 3.3 and 3.4. The parameter values and choices for a and h_f are the same as those used in the computation of the steady-state profiles in figure 7, and steady-state profiles based on the solution of (3.60) and (3.63) are plotted in figure 9(c).

The main unresolved issue relating to these steady-state profiles was whether they were stable. Recall that a simple mass-balance argument suggests that the smaller steady profile, shown as a dashed line in figure 9(c), should be unstable, while the larger profile should be stable. Our numerical solutions do indeed suggest that this is the case: the solution in figure 9(a) is based on an initial ice sheet close in shape to but slightly smaller than the dashed profile in figure 9(c). As suggested by the argument at the end of § 3.4, the ice sheet evolves away from this initial profile. In fact, numerically, the ice sheet again shrinks to zero size in finite time. Meanwhile the solution shown in figure 9(b) has an initial shape which is close to but slightly larger than the dashed steady-state solution in figure 9(c) In this case, the ice sheet grows until it relaxes to a steady surface profile close to that shown as a solid line in figure 9(c), which we had previously speculated to be stable.

Clearly, these results lend some weight to the stability argument of § 3.4, and also indicate that the reduced model (3.52)–(3.55) captures the behaviour of (2.12), (2.13) for small ε. Further support for our asymptotic results is provided by the numerically computed ice fluxes at the grounding line, which closely match the form of q_g predicted by our asymptotic results (figure 10).

5. Discussion

This paper has been concerned with finding boundary conditions for marine ice sheets. The basic problem addressed is the following (see also Wilchinsky 2001).

In order to construct a well-posed model for a marine ice sheet with a moving margin, two independent boundary conditions are required at the grounding line. One condition on the ice thickness arises naturally from the fact that the grounding line represents the location where the ice becomes afloat. Hence the ice thickness at the grounding line is fixed by the depth of the sea floor. This leaves a second condition to be determined.

Notwithstanding claims to the contrary in e.g. Hindmarsh (1996, equation (4)), this second condition cannot be found by simply rewriting the parabolic partial differential equation for the ice thickness in the ice-sheet interior; this procedure does not introduce additional information into the problem. Instead, the second boundary condition must be found by solving a boundary-layer problem which describes the transition from ice-sheet to ice-shelf flow.

In this paper, we have considered the case of a two-dimensional ice sheet which slides rapidly over its bed. The friction τ_b at the base of the ice is assumed to be related to the sliding velocity u by a power-law relationship of the form $\tau_b = C|u|^{m-1}u$ with $m > 0$. Our analysis of the relevant boundary-layer problem has yielded two principal results, as follows.

(i) If the axial deviatoric stresses in the grounded part of the ice sheet are negligible then the ice thickness at the grounding line must be small compared with the ice thickness in the interior of the ice sheet. This is necessary if ice fluxes at the grounding line are to match ice fluxes upstream of the grounding line (see §3.3). If the ice thickness at the grounding line is comparable with the ice thickness inland, rapid retreat of the grounding line ensues (§§3.2 and 4). Asymptotically, this result requires zero ice thickness at leading order at the grounding line, for ice sheets which evolve in their interior on the same time scale as that at which their grounding lines migrate. Zero marginal ice thickness then replaces the flotation condition that is usually applied.

(ii) The ice flux at the grounding line can be related to the ice thickness and hence to the depth of the sea floor below sea level at the grounding line. This provides the required second boundary condition. As may be expected physically, the ice flux is an increasing function of the sea-floor depth. Equation (3.55) gives a good approximation for this flux and can be written in dimensional terms as

$$q(x_g, t) = \left(\frac{A(\rho g)^{n+1}(1 - \rho/\rho_w)^n}{4^n C} \right)^{1/(m+1)} h^{(m+n+3)/(m+1)}. \tag{5.1}$$

The first of these boundary conditions is somewhat surprising, especially as the ice-sheet bed in parts of West Antarctica is over a kilometre below sea level. However, as demonstrated in §3.1, it is a necessary result of imposing the asymptotic limit $\varepsilon \ll 1$. In fact, the only way in which vanishing ice thickness at the grounding line can be avoided is if δ is also small, with $\delta \sim \varepsilon$. The relevant treatment of that limit is sketched in the appendix. (Physically, the fact that parts of the Antarctic ice sheet are grounded well below sea level also raises the question whether a grounding-line retreat into these areas could precipitate a rapid and irreversible disintegration of the ice sheet, as our results would suggest. One can also speculate whether the original growth of the West Antarctic Ice Sheet occurred when the ice-sheet bed was rather less deep, having subsequently been deepened by isostatic depression and glacial erosion.)

Qualitatively, the second boundary condition is of the same form as that used by Oerlemans (2002), in the sense that it predicts a flux increasing with ice thickness, with implications for ice-sheet stability that are discussed below. The boundary condition

is also similar to that predicted previously by Chugunov & Wilchinsky (1996) and subsequently used by Wilchinsky (2001) in his study of ice-sheet stability.

There is, however, a caveat: the reason why it is possible to relate ice flux to ice thickness at the grounding line is that the axial deviatoric stress, $2A^{-1/n}h|u_x|^{1/n-1}u_x$ in dimensional terms, can be related directly to the ice thickness through the second (stress) boundary condition in (2.6). This, in turn, is the case because the spatially one-dimensional ice-shelf equation (2.2) combined with the first boundary condition in (2.5) can be integrated explicitly to yield the second equality in (2.6) (by one-dimensional we mean here that there is one independent spatial variable, x; of course the shelf itself is two-dimensional, as mentioned earlier).

When considering a two-dimensional analogue of $(2.2a, b)$, the same force-balance result no longer applies, and the ice sheet can no longer be uncoupled from the ice shelf. This effect is known as 'buttressing' in glaciology (e.g. MacAyeal 1987), a term also used to describe the sea phenomenon whereby floor protrusions make contact with the base of a floating shelf (e.g. Dupont & Alley 2005*b*). A number of heuristic ways to parameterize the effect of a three-dimensional ice shelf (involving two independent spatial variables) have been devised (see e.g. Dupont & Alley 2005*a*). Generally, a three-dimensional ice shelf, confined to an embayment as is typically true of large ice shelves, is assumed to reduce the axial deviatoric stress at the grounding line compared with the value predicted by $(2.6a, b)$. It is however unclear whether a simple correction factor such as that used for instance by Dupont & Alley (2005*a*), which would correspond to a simple reduction in the parameter δ in the scaled boundary condition (2.14), can adequately account for this, as the extent of buttressing is likely to depend critically on the length of the ice shelf.

Given this caveat, a number of interesting fundamental questions can nevertheless be addressed using our simple, spatially one-dimensional, depth-integrated model. Firstly, our model shows that, for a given accumulation rate, two-dimensional marine ice sheets have a discrete number of steady surface profiles for which the constraint (3.60) is satisfied. This result, which confirms a similar one by Wilchinsky (2001), stands in contrast with some numerical results recently obtained by Vieli & Payne (2005) and Pattyn *et al.* (2006). These authors have found that a steady grounding-line position in their models is sometimes neutrally stable to small perturbations. This occurs in particular when the extent of the boundary layer between sheet flow and shelf flow in their models is narrow, and it also appears to depend on the numerical method chosen for tracking the grounding line as a free boundary. One likely explanation is that the boundary layer is not resolved numerically by the relatively coarse grids employed in their numerical work.

If ice sheets indeed admit a discrete set of steady surface profiles, this raises the question whether these surface profiles are stable. A complete answer to this question is beyond the scope of the present paper. Nonetheless, the simple mass-balance argument in §3.4 suggests that stability is controlled by bed slope: on the basis of this argument, a stable two-dimensional steady marine ice sheet requires its margin to be located on a sufficiently steep downward bed slope.

A number of interesting questions are still outstanding. A stability analysis for the steady marine ice-sheet problem of §3.4 is desirable in order to determine whether the stability criterion (3.66) is valid. Given this criterion, a consideration of ice sheets whose bed deforms under the weight of the overlying ice (e.g. Wilchinsky & Feltham 2004) becomes of interest, as bed deformation is likely to affect bed slopes at the ice-sheet margin (as is glacial erosion). More generally, the extension of the present

work to ice sheets which are not sliding rapidly is of significant interest, and this will form the subject of a companion paper currently in preparation.

At a more physical level, there are numerous other complications to be addressed. As predicted by our boundary-layer model, it is generally true that ice velocities near the grounding line of marine ice sheets are fast, but this rapid ice flow is usually channelized into ice streams (e.g. Alley & Bindschadler 2001), which are narrow bands of rapidly flowing ice. This could change the boundary-layer problem significantly, and an important effect then to take into account is that rapid sliding may in fact be poorly described by a power law, as assumed in this paper, and may more closely follow a Coulomb-type friction law (Iverson *et al.* 1999; Tulaczyk 1999; Schoof 2004, 2005, 2006*a*, *b*). In any case, pore water pressures at the base of the ice sheet are likely to play an important role in the flow of these ice streams, and temporal variations in sliding due to the melting and freezing of pore-water at the base of the ice may also become important (e.g. Fowler & Johnson 1996; Tulaczyk, Kamb & Engelhardt 2000). Moreover, the effect of tides on the flow of ice in the sheet–shelf transition zone is observed to cause stick–slip behaviour at the base of the ice, but the physical mechanisms involved and their effect on the flow of the ice sheet over long time scales are poorly understood (e.g. Anandakrishnan *et al.* 2003; Weertman 2005). Future work will need to address these challenges.

Appendix A. The limit $\delta \sim \varepsilon \ll 1$

In the main part of this paper, we have treated δ as an $O(1)$ parameter, though realistically δ is ~ 0.1 and so can be treated as small, so that the relative ordering of ε and δ becomes important. Below, we sketch the case $\varepsilon \sim \delta \ll 1$ (or more pertinently, $\varepsilon \sim \delta/8$), as this permits $O(1)$ ice thicknesses h_f at the grounding line and the matching of fluxes with the interior of the ice sheet. In practice, this limit requires $\varepsilon \approx 10^{-2}$, which in turn is possible only for very cold ice (for which A in (2.8) becomes smaller) and for large sliding velocities $[u]$.

The boundary conditions (2.14) can be written as

$$h = h_f, \qquad u_x = \left(\frac{\delta h_f}{8\varepsilon}\right)^n, \qquad \text{at } x = x_g(t). \tag{A 1}$$

As we shall demonstrate, a boundary layer is no longer required when $\delta \sim 8\varepsilon$, and a Stefan-type condition determining the rate of grounding-line migration can be computed directly. Taking the total derivative of the first equality in (A 1) with respect to t yields

$$h_t + h_x \dot{x}_g = h_{fx} \dot{x}_g, \tag{A 2}$$

where $\dot{x}_g = \mathrm{d}x_g/\mathrm{d}t$ and h_t as well as h_x are the relevant boundary values at $x = x_g$. Moreover $h_{fx} = \partial h_f/\partial x$. From (3.1), (3.3) and (A 1), we have at $x = x_g$

$$h_t = a - u h_x - u_x h = a + h_f^{1/m}|(h-b)_x|^{1/m-1}(h-b)_x h_x - (\delta/8\varepsilon)^n h_f^{n+1}. \tag{A 3}$$

Eliminating h_t between (A 2) and (A 3) finally yields

$$(h_f - h)_x \dot{x}_g = a + h_f^{1/m} |(h-b)_x|^{1/m-1} (h-b)_x h_x - (\delta/8\varepsilon)^n h_f^{n+1} \qquad \text{(A 4)}$$

as the required Stefan condition, which serves as one boundary condition for the diffusion problem (3.3) at $x = x_g$. The other boundary condition is naturally the flotation condition $h = h_f$. A similar boundary condition may be found in Thomas & Bentley (1978).

Below, we show that the free-boundary condition (A 4) is consistent with the results in §3.3 in the appropriate limit, $\varepsilon \ll \delta \ll 1$. Recall that in §3.3, we considered the case of small ε with $\delta = O(1)$. Next, we show that (3.51) corresponds not only to taking the limit of small H_f in (3.39)–(3.41) but also to the limit of small δ (i.e. the limit $\varepsilon \ll \delta \ll 1$). Subsequently, we show that the same equation can also be obtained from (A 4) by taking the same limit (so that $\varepsilon \ll \delta$ in (A 4)).

A.1. *The limit $\delta \ll 1$ in (3.39)–(3.41)*

When $\delta \ll 1$ in (3.39)–(3.41), the following rescaling becomes appropriate:

$$U = \delta^{n/(m+1)} U', \qquad X = \delta^{-mn/(m+1)} X'. \qquad \text{(A 5)}$$

The boundary-layer problem (3.39)–(3.41) then becomes

$$\left. \begin{array}{c} 4\delta(H|U'_{X'}|^{1/n-1} U'_{X'})_{X'} - |U'|^{m-1} U' + H H_{X'} = 0 \\ (U'H)_{X'} = 0 \\ H \geqslant H_f \end{array} \right\} \text{ on } X' \in (0, \infty), \quad \text{(A 6a,b)}$$

$$\left. \begin{array}{c} H = H_f \\ |U'_{X'}|^{1/n-1} U'_{X'} = -H_f/8 \end{array} \right\} \text{ at } X' = 0 \qquad \text{(A 7)}$$

together with $U' \to 0$, $\delta^{n/(m+1)} U'H \to Q$, as $X' \to \infty$. Ignoring the $O(\delta)$ term in (A 6a) gives the lubrication relation

$$U' = H^{1/m} |H_{X'}|^{1/m-1} H_{X'}, \qquad \text{(A 8)}$$

while (A 6b) gives

$$U' H_{X'} + U'_{X'} H = 0. \qquad \text{(A 9)}$$

Using this last equation at $X' = 0$ with the boundary conditions (A 7) and (A 8) yields

$$|H_{X'}|^{1/m+1} = 8^{-n} H_f^{n+1-1/m}, \qquad \text{(A 10)}$$

where the inequality in (A 6) further ensures that $|H_{X'}| = H_{X'} \geqslant 0$ at the grounding line $X' = 0$. Substituting this into (A 8) gives, at $X' = 0$,

$$U' H = \frac{H_f^{m+n+3/(m+1)}}{8^{n/(m+1)}}. \qquad \text{(A 11)}$$

By (A 6b), $U'H$ remains constant for X' finite. Hence matching gives $Q = UH = \delta^{n/(m+1)} U'H = (\delta/8)^{n/(m+1)} H_f^{(m+n+3)/(m+1)}$ as the flux relation for the outer problem, which is the same as (3.51).

It is then apparent that $Q \sim O(\delta^{n/(m+1)})$ if $H_f \sim O(1)$ and that an $O(1)$ flux requires $H_f = O(\delta^{-n/(m+n+3)})$ (which implies that $h_f \sim (\varepsilon/\delta)^{-n/(m+n+3)}$). Without going into details, we note that the derivation above carries over to this case under the rescaling $H' = \delta^{-n/(m+n+3)} H$, $H'_f = \delta^{-n/(m+n+3)} H_f = (\varepsilon/\delta)^{-n/(m+n+3)} h_f$, again provided that $\varepsilon \ll \delta \ll 1$ and that (3.51) remains valid.

A.2. *The limit $\varepsilon \ll \delta$ in (A 4)*

When $\varepsilon \ll \delta$, the last paragraph in §A.1 above suggests that h_f should in fact be of order $(\varepsilon/\delta)^{n/(n+m+3)}$. We rescale as follows:

$$h = (\varepsilon/\delta)^{n/(n+m+3)}H, \qquad h_f = (\varepsilon/\delta)^{n/(n+m+3)}H_f, \\ b = (\varepsilon/\delta)^{n/(n+m+3)}B, \qquad x = (\varepsilon/\delta)^{n(m+2)/(n+m+3)}X, \quad (A\,12)$$

the last rescaling being motivated by the distance rescaling in §3.3. As in §3.3, we again suppose that the outer $(x-)$ length scale is the scale over which bed topography varies, and retain B_x and $H_{fx} = (1-\delta)^{-1}B_x$ as the relevant bed and flotation slopes (rather than B_X and H_{fX}). Then (A 4) becomes

$$\left(\frac{\varepsilon}{\delta}\right)^{n/(n+m+3)}\left(H_X - \left(\frac{\varepsilon}{\delta}\right)^{n(m+2)/(n+m+3)}H_{fx}\right)\dot{x}_g$$

$$= \left(\frac{\varepsilon}{\delta}\right)^{n(m+2)/(n+m+3)}a + H_f^{1/m}\left|H_X - \left(\frac{\varepsilon}{\delta}\right)^{n(m+2)/(n+m+3)}B_x\right|^{1/m-1}$$

$$\times\left(H_X - \left(\frac{\varepsilon}{\delta}\right)^{n(m+2)/(n+m+3)}B_x\right)H_x - \frac{H_f^{n+1}}{8^n}. \qquad (A\,13)$$

Ignoring higher-order terms in ε/δ,

$$H_f^{1/m}|H_x|^{1/m+1} = H_f^{n+1}/8^n. \qquad (A\,14)$$

Using the fact that bed slopes are assumed small, as explained above, we have $Q = h^{1/m+1}|h_x|^{1/m-1}h_x|_{x=x_g} = H_f^{1/m+1}|H_X|^{1/m-1}H_X|_{X=0}$ and finally obtain the desired result,

$$q = \frac{H_f^{(m+n+3)/(m+1)}}{8^{n/(m+1)}}. \qquad (A\,15)$$

Thus the two determinations of flux in the limit $\varepsilon \ll \delta \ll 1$ agree.

REFERENCES

ALLEY, R. B. & BINDSCHADLER, R. A. (ed.) 2001 *The West Antarctic Ice Sheet: Behaviour and Environment*. American Geophysical Union, Washington, DC.

ANANDAKRISHNAN, S., VOIGT, D. E., ALLEY, R. B. & KING, M. A. 2003 Ice stream flow speed is strongly modulated by the tide beneath the Ross Ice Shelf. *Geophys. Res. Letts.* **30**, doi: 10.1029/2002GL016329.

BUELER, E., LINGLE, C. S., KALLEN-BROWN, J. A., COVEY, D. N. & BOWMAN, L. N. 2005 Exact solutions and verification of numerical models for isothermal ice sheets. *J. Glaciol.* **51** (173), 291–306.

CALVO, N., DÍAZ, J., DURANY, J., SCHIAVI, E. & VÁZQUEZ, C. 2002 On a doubly nonlinear parabolic obstacle problem modelling ice sheet dynamics. *SIAM J. Appl. Maths* **63**, 683–707.

CHUGUNOV, V. A. & WILCHINSKY, A. V. 1996 Modelling of marine glacier and ice-sheet–ice-shelf transition zone based on asymptotic analysis. *Ann. Glaciol.* **23**, 59–67.

CRANK, J. 1984 *Free and Moving Boundary Problems*. Clarendon.

DUPONT, T. K. & ALLEY, R. B. 2005a Assessment of the importance of ice-shelf buttressing to ice sheet flows. *Geophys. Res. Letts.* **32** (L04503), doi:10.1029/2004GL022024.

DUPONT, T. K. & ALLEY, R. B. 2005b Conditions for the reversal of ice/air surface slope on ice streams and ice shelves: a model study. *Ann. Glaciol.* **40**, 139–144.

FOWLER, A. C. 1977 Glacier dynamics. PhD thesis, Oxford University.

FOWLER, A. C. 1981 A theoretical treatment of the sliding of glaciers in the absence of cavitation. *Phil. Trans. R. Soc. Lond.* **298** (1445), 637–685.

FOWLER, A. C. 1982 Waves on glaciers. *J. Fluid Mech.* **120**, 283–321.

Fowler, A. C. 1997 *Mathematical Models in the Applied Sciences*. Cambridge University Press.

Fowler, A. C. 2001 Modelling the flow of glaciers and ice sheets. In *Continuum Mechanics and Applications in Geophysics and the Environment* (ed. B. Straughan, R. Greve, H. Ehrentraut & Y. Wang), pp. 276–304. Springer.

Fowler, A. C. & Johnson, C. 1996 Ice-sheet surging and ice-stream formation. *Ann. Glaciol.* **23**, 68–73.

Fowler, A. C. & Larson, D. A. 1978 On the flow of polythermal glaciers. I. Model and preliminary analysis. *Proc. R. Soc. Lond.* A **363**, 217–242.

Fowler, A. C. & Larson, D. A. 1980 The uniqueness of steady state flows in glaciers and ice sheets. *Geophys. J. R. Astron. Soc.* **63**, 347–359.

Herterich, K. 1987 On the flow within the transition zone between ice sheet and ice shelf. In *Dynamics of the West Antarctic Ice Sheet. Proc. Workshop held in Utrecht, May 6–8, 1985* (ed. C. J. van der Veen & J. Oerlemans), pp. 185–202. D. Reidel.

Hindmarsh, R. C. A. 1996 Stability of ice rises and uncoupled marine ice sheets. *Ann. Glaciol.* **23**, 94–104.

Hindmarsh, R. C. A. 2006 The role of membrane-like stresses in determining the stability and sensitivity of the antarctic ice-sheets: back-pressure and grounding-line motion. *Phil. Trans. R. Soc. Lond.* A **364**, 1733–1767.

Hindmarsh, R. C. A. & LeMeur, E. 2001 Dynamical processes involved in the retreat of marine ice sheets. *J. Glaciol.* **47** (157), 271–282.

Hutter, K. 1983 *Theoretical Glaciology*. D. Reidel.

Iverson, N. R., Baker, R. W., Hooke, R. LeB., Hanson, B. & Jansson, P. 1999 Coupling between a glacier and a soft bed: I. A relation between effective pressure and local shear stress determined from till elasticity. *J. Glaciol.* **45** (149), 31–40.

LeMeur, E. & Hindmarsh, R. C. A. 2001 Coupled marine ice-sheet/earth dynamics using a dynamically consistent ice sheet and a self-gravitating viscous earth model. *J. Glaciol.* **47** (157), 258–270.

MacAyeal, D. R. 1987 Ice-shelf backpressure: form drag versus dynamics drag. In *Dynamics of the West Antarctic Ice Sheet. Proc. Workshop held in Utrecht, May 6–8, 1985* (ed. C. J. van der Veen & J. Oerlemans), pp. 141–160. D. Reidel.

MacAyeal, D. R. 1989 Large-scale flow over a viscous basal sediment: theory and application to Ice Stream E, Antarctica. *J. Geophys. Res.* **94** (B4), 4017–4087.

MacAyeal, D. R. 1996 EISMINT: Lessons in Ice-Sheet Modeling. *Tech. Rep.* Department of Geophysical Sciences, University of Chicago, unpublished lecture notes.

MacAyeal, D. R. & Barcilon, V. 1988 Ice-shelf response to ice-stream discharge fluctuations: I. Unconfined ice tongues. *J. Glaciol.* **34** (116), 121–127.

Morland, L. W. 1987 Unconfined ice-shelf flow. In *Dynamics of the West Antarctic Ice Sheet. Proc. Workshop held in Utrecht, May 6–8, 1985* (ed. C. J. van der Veen & J. Oerlemans), pp. 99–116. D. Reidel.

Morland, L. W. & Johnson, I. R. 1980 Steady motion of ice sheets. *J. Glaciol.* **25** (92), 229–246.

Muszynski, I. & Birchfield, G. E. 1987 A coupled marine ice-stream–ice-shelf model. *J. Glaciol.* **33** (113), 3–15.

Nye, J. F. 2000 A flow model for the polar caps of Mars. *J. Glaciol.* **46** (154), 438–444.

Oerlemans, J. 2002 Global dynamics of the Antarctic ice sheet. *Climate Dyn.* **19**, 85–93.

Paterson, W. S. B. 1994 *The Physics of Glaciers*, 3rd edn. Pergamon.

Pattyn, F., Huyghe, A., De Brabander, S. & De Smedt, B. 2006 Role of transition zones in marine ice sheet dynamics. *J. Geophys. Res.* **111** (F02004), doi:10.1029/2005JF000394.

Schoof, C. 2004 On the mechanics of ice stream shear margins. *J. Glaciol.* **50** (169), 208–218.

Schoof, C. 2005 The effect of cavitation on glacier sliding. *Proc. R. Soc. Lond.* A **461**, 609–627, doi:10.1098/rspa.2004.1350.

Schoof, C. 2006a A variational approach to ice-stream flow. *J. Fluid Mech.* **556**, 227–251.

Schoof, C. 2006b Variational methods for glacier flow over plastic till. *J. Fluid Mech.* **555**, 299–320.

Shumskiy, P. A. & Krass, M. S. 1976 Mathematical models of ice shelves. *J. Glaciol.* **17**, 419–432.

Thomas, R. H. & Bentley, C. R. 1978 A model for Holocene retreat of the West Antarctic ice sheet. *Quat. Res.* **10**, 150–170.

Tulaczyk, S. 1999 Ice sliding over weak, fine-grained till: dependence of ice–till interactions on till granulometry. *Spec. Paper Geol. Soc. Am.* **337**, 159–177.

Tulaczyk, S., Kamb, W. B. & Engelhardt, H. F. 2000 Basal mechanisms of Ice Stream B, West Antarctica: 2. Undrained plastic bed model. *J. Geophys. Res.* **105** (B1), 483–494.

van der Veen, C. J. 1985 Response of a marine ice sheet to changes at the grounding line. *Quat. Res.* **24**, 257–267.

Vieli, A. & Payne, A. J. 2005 Assessing the ability of numerical ice sheet models to simulate grounding line migration. *J. Geophys. Res.* **110** (F01003), doi:10.1029/2004JF000202.

Weertman, J. 1974 Stability of the junction of an ice sheet and an ice shelf. *J. Glaciol.* **13** (67), 3–13.

Weertman, J. 2005 Slip event propagation direction in transition region of low surface slope. *Ann. Glaciol.* **40**, 43–46.

Weis, M., Greve, R. & Hutter, K. 1999 Theory of shallow ice shelves. *Cont. Mech. Thermodyn.* **11**, 15–50.

Wilchinsky, A. V. 2001 Studying ice sheet stability using the method of separation of variables. *Geophys. Astrophys. Fluid Dyn.* **94**, 15–45.

Wilchinsky, A. V. & Chugunov, V. A. 2000 Ice stream-ice shelf transition: theoretical analysis of two-dimensional flow. *Ann. Glaciol.* **30**, 153–162.

Wilchinsky, A. V. & Chugunov, V. A. 2001 Modelling ice flow in various glacier zones. *J. Appl. Maths Mech.* **65**, 479–493.

Wilchinsky, A. V. & Feltham, D. L. 2004 Stability of an ice sheet on an elastic bed. *Eur. J. Mech. B/Fluids* **23**, 681–694.